J. Mater. Chem. A
Journal of Materials Chemistry A
Dynamic Article Links ►
Cite this: DOI: 10.1039/c0xx00000x
www.rsc.org/xxxxxx

COMMUNICATION

Directional size-triggered microdroplet target transport on gradient-step fibers

Yan Xue,[a] Yuan Chen,[a] Ting Wang,[a] Lei Jiang[b] and Yongmei Zheng*[a]

Received (in XXX, XXX) Xth XXXXXXXXX 20XX, Accepted Xth XXXXXXXXX 20XX
DOI: 10.1039/b000000x

We present a unique size-triggered microdroplet target transport achieved on gradient-step spindle-knot fibers (GSFs). GSFs are fabricated controllably by developing a velocity-changed coating method, the gradient features of which can be unidirectional, middle and two-side symmetric spindle-knots modes to modulate droplet target transport in directions. This finding offers an insight into how to control effectively liquid self-transport in directions for water collection, which may be also extended into realms of smart materials contributed to fluid-controlling.

Directional movement of droplet or droplet self-running with little energy has been payed much attention into fundational and technological researches for promising applications, e.g., operation of microfluidic, biological analysis devices, fog capturing and condensers[1–5]. This directional transport is usually controlled by the well-designed physical or chemical gradient onto surfaces[5]. Up to now, it is how to design a kind of unique structured surface to control effectively the micro-droplet transport in directions in a long range that is still challenging. Recently, biological surfaces, e.g., conical spines[6–9] of cactus and spindle-knots of spider silk[10–13], smartly control droplet transport via gradient of micro- and nanostructures[6,10]. It has aroused interests in designing carefully the fluid-collecting surfaces[11–19]. Inspired by water collecting properties on either the cactus spines with geometric gradient or the wetted spider silk with rough curve spindle-knots, the structured fiber can be designed considerably[6]. Here, we present the unique size-triggered microdroplet target transport on gradient-step spindle-knot fibers (GSFs) that are designed carefully and fabricated controllably by a velocity-changed coating method. We obtain the different styles of fibers including unidirectional size-increasing spindle-knots mode, middle and two-side symmetric modes in sizes of spindle-knots via controlling the changes of drawing velocities. We investigate that the uni-direction gradient mode in length range how to allow droplets to achieve a target transport in directions, in addition to middle or two-side symmetric size spindle-knots modes for droplet transport in aggregation or separation in contrasting directions. Besides, in dynamic transport process, the transport velocity of droplet is estimated when droplet pass along not only a serials gradient-step spindle-knots but also a single spindle-knot. The mechanism will be elucidated based on size effect to combine the continuous capillary gradient cooperative effect in coalescence of droplets. This finding opens a way via little energy to effectively control liquid self-transport in directions, which may be also extended into relams of smart materials contributed to fluid-controlling.

To obtain GSFs, the velocity-changed coating method is used firstly (as illustrated in **Figure 1**a). An original fiber is dipped in a polymer solution reservoir, and then fiber is drawn out horizontally by the changeable-controlled velocity, thus a cone film covers over original fiber (see supplementary Fig. S1). Fig. 1b shows the optical images of in- situ GSF formation, which is recorded by high speed charge-coupled device (CCD). When the nylon fiber (e.g., ~ 110 μm in diameter) is drawn out from the

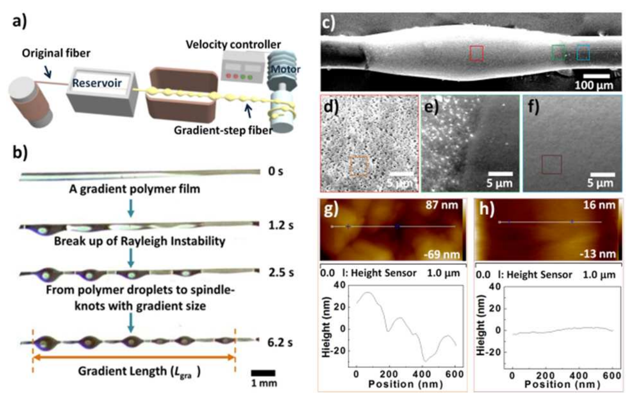

Fig. 1 Fabrication of gradient-step spindle-knot fibers (GSFs) and their microstructure. (a) Illustration of the method to fabricate GSFs. A main-fiber is drawn out from polymer solution via a changing velocity by a motor connected with a velocity controller, then dried at the temperature drier for 90 s, and the well-formed fiber is collected. (**b**) Optical images of in-situ observation on process of fiber fabrication with time. A gradient solution film forms on the fiber, initially (0 s), then the film is unstable and the prototype of bigger droplets emerges due to Rayleigh instability at ~ 1.2 s. Gradient-size droplets begin to form at ~ 2.5 s, and continuous gradient-sized droplets form finally at ~ 6.2 s. The gradient length (L_{gra}) is defined as the maximum segment of gradient from smallest spindle-knot to biggest spindle-knot (see orange dual-arrows). **(c-f)** SEM images of a spindle knot on a fiber with magnified pictures of spindle center (a more rough structure (c)), joint (a smooth structure (f)) and the connecting of spindle and joint (d). **(g-h)** AFM images of spindle and joint. Spindle with mean roughness Ra=14.2 nm, the vertical distance between top and base h=68.1 nm (g, the inset); joint with Ra=0.3 nm, h=5.75 nm (h, the inset).

solution of poly(methyl methacrylate) (PMMA) in *N,N*-dimethylformamide (DMF) (10 wt%), via changing velocities from initial velocity (V_0 ~ 0 mm/s) to terminal velocity (V_t ~ 21.4 mm/s) with constant accelerated speed a = 8.3 mm/s^2, a cone-gradient solution film (with an increasing thickness) covers over nylon fiber. After a short time (~ 1.2 s), the cone solution film appears convex-concave immediately, subsequently, inducing that periodic polymer droplets with gradient-step height (i.e., ~ 208.8 ± 44.0 μm at minimum, ~ 595 ± 71.3 μm at maximum) (at ~ 2.5 s). In terms of report by Plateau[20], the axisymmetric wavelengths larger than the circumference 2π (r+h) of the fluid cylinder are unstable (r is the radius of fiber, h is the thickness of film), and the Laplace pressure is difference between thicker film and thinner one[17,21], which contributes to break-up of film. According to the law of Rayleigh Instability[22], the periodicity and the size of the polymer droplets are determined by the thickness of the solution film that further regulated by the capillary number (*Ca*) as follows: $Ca = \eta V/\gamma$, where η is the solution viscosity; V is the drawing velocity and γ is the solution surface tension. The thickness of film depends on the velocity of fiber withdraw rate [23–25]. In our fabrication, thickness of polymer film is controlled carefully in gradient by the drawing changable velocity. A gradient Rayleigh instability is carried out the break-up of a cone liquid film into gradient-stepped droplets (see supplementary Fig. S1-3), which offer a way to achieve a unique GSF. In addition to geometry effect along a serial gradient-size spindle-knots, local gradient on microstructures in details are observed by the scanning electron microscopy (SEM) and atomic force microscopy (AFM). Fig. 1c-f show SEM images of the local gradient morphology on spindle-knot with strong porous structure at centre of spindle-knot (Fig. 1d) and gradient porous structure at middle (Fig. 1e), and relative smooth structure at the side (Fig. 1f). Fig. 1g-h show AFM images of roughness on centre of spindle-knot with the mean roughness Ra=14.2 nm (with vertical distance between the top and base of spindle h = 68.1 nm) (Fig. 1g) and at side of spindle-knot with Ra=0.3 nm (with h = 5.75 nm) (Fig. 1h), respectively. Each spindle-knot can be roughness in gradient, which is similar to that of wetted spider silks. As for GSF, it has thereby gradient-step spindle- knots in a relative long range, which becomes a unique structure.

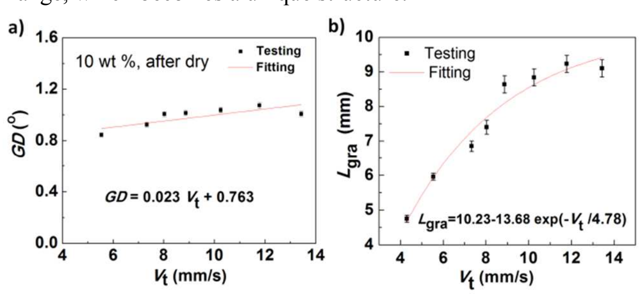

Fig. 2 The relationship of gradient degree (*GD*) and gradient length (L_{gra}) of GSF versus drawing velocity (V_t). **(a)** The relationship of *GD* versus V_t after dry at 10 wt % solution. There is $GD = 0.023\ V_t + 0.763$ by data fitting, where *GD* is defined as arctangent, i.e., the ratio of altitude biggest-smallest spindle-knot difference to gradient length L_{gra}. **(b)** Relationship of V_t versus L_{gra}. The L_{gra} increases sharply with the V_t ranged in ~ 4–8 mm/s. The L_{gra} increases slowly with V_t ranged in ~ 9–14 mm/s. An extreme L_{gra} ≈ 8.96 ± 0.25 mm at V_t ~ 12 mm/s. There is L_{gra} =10.23–13.68 exp (–V_t /4.78) (mm) by data fitting (see red lines).

Features of GSFs are related to drawing velocities and the concentrations of solution (see supplementary Fig. S2). The gradients are kept along the GSF, where the heights would be shortened to ~ 30–45 % as polymer droplets changes into spindle-knots after dry, but their widths and pitches are still little changed (see supplementary Fig. S3). We define gradient degree (*GD*) as arctangent the ratio of altitude difference (between the largest and the smallest knot) to gradient length (L_{gra}). **Figure 2**a shows the relationship between *GD* and V_t for the samples fabricated at the 10 wt% (concentration) after dried. These GSFs maintain the *GD* ~ 0.8°–1.1°. There is linear relationship: $GD = 0.023\ V_t + 0.763$ by fitting. It indicates an increasing V_t would induce an increasing *GD*. The relationship between V_t at maximum and L_{gra} are shown in Fig. 2b, it is L_{gra} =10.23–13.68

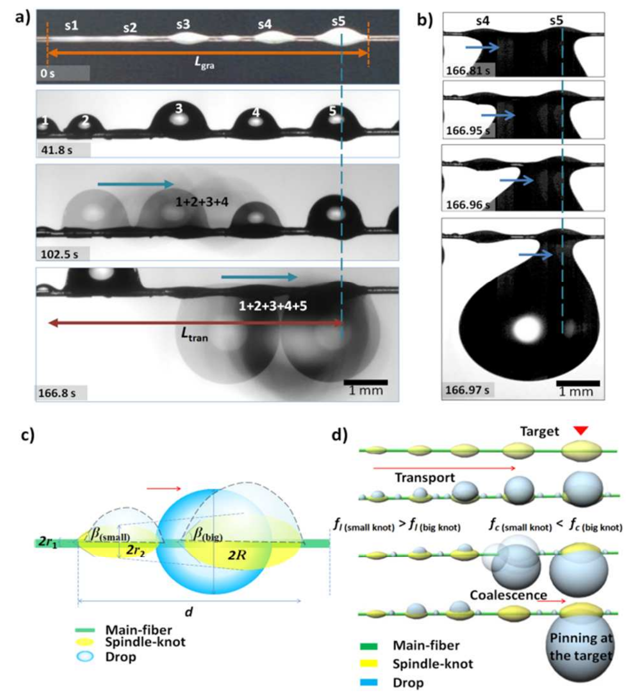

Fig. 3 Droplet target transport on GSF and illustration of its mechanism. **(a)** Optical images of droplet target transport on GSF with uni-direction gradient mode. Droplet transport is observed on GSF with five spindle-knots (marked with s1, s2, s3, s4, s5) from small to big in size with L_{gra} = ~ 7.35 mm (see red dual-arrow). At ~ 41.8 s, droplet 1 and 2 tends to coalesce toward point s1. Subsequently, droplet (1+2), droplet 3 and droplet 4 coalesce directionally into droplet (1+2+3+4) at ~ 102.5 s, reaching point s4 passing s2 and s3. Finally, droplets coalesce into droplet (1+2+3+4+5), reaching point s5 the biggest spindle-knot at ~ 166.8 s via the transport length (s1→s2→s3→s4→s5) of ~ 6.6 mm. The transport length (L_{tran}) is defined as the distance of the droplet mass-center moving. Scale bar is 1 mm. **(b)** Droplet transport is continuous from bigger spindle-knot at s4 to biggest one at s5 quickly in ~ 166.81–166.96 s, and destination on point s5 at ~ 166.97 s, with a maximum volume of ~ 188.7 μl. **(c)** Illustration of the parameters, where r is the local radius, R is the droplet radius, β is the half apex-angles of the spindle-knots, d is the distance between two adjacent spindle-knots outer ends. **(d)** Illustration of mechanism. As the Laplace pressure $f_{l\ (small\ knot)} > f_{l\ (big\ knot)}$ and capillary adhesion force $f_{c\ (small\ knot)} < f_{c\ (big\ knot)}$, a continuous gradient capillary cooperative forces drive the droplets transport from small to big spindle-knot. Red arrows indicate the direction of droplet transport.

exp ($-V_t$/4.78) (mm) by fitting, indicating the L_{gra} increases sharply with increasing of V_t, while slowly at V_t > 8 mm/s. There exists $L_{gra, max}$ ≈ 8.96 ±0.25 mm at maximum until V_t ~ 13.5 mm/s at maximum, indicating the L_{gra} can be further effectively regulated by controlling the V_t. From analysis above, the GSF possess the continuous gradient-step spindle-knots along fiber (including local gradient along spindle-knot) and integrates effectively a unique gradient-structure cooperation effect, which favour water collection in efficiency.

We observe the property of microdroplet target transport on GSFs. **Figure 3**a shows the optical images of droplet transport process on GSF with uni-direction gradient mode composed of five increasing-sized spindle-knots (marked with s1, s2, s3, s4, s5) with L_{gra} ~ 7.35 mm. The humidity of 90% is provided onto GSF via an ultrasonic humidifier. The initial state before water condensed is defined as 0 s. After ~ 41.8 s, we see five water droplets (numbered with 1, 2, 3, 4, 5) on GSF. Continuously, water droplets 1, 2 coalesce directionally into droplet (1+2) reaching point s1. Subsequently, droplet (1+2), droplet 3 and 4 coalesce directionally into droplet (1+2+3+4) at ~ 102.5 s, reaching point s4 passing s2 and s3. Finally, droplets coalesce into droplet (1+2+3+4+5), reaching point s5 at the biggest spindle-knot. The droplets move from small spindle-knot (point s1) to big one (point s5), via the transport length (s1→s2→s3→s4→s5) of ~ 6.6 mm. Fig. 3b shows the dynamic details of the droplet transport toward the location of the biggest spindle-knot as target at time, where the droplet is formed at two adjacent spindles (at ~ 166.81 s), and finally transports from the bigger one (at point s4) to the biggest one (at point s5) quickly (at ~ 166.95–166.97 s), and targets destination on point s5 at ~ 166.97 s, with critical volume of ~ 23.6 µl. In the process, the three-phase contact line decreases sharply (at ~ 166.81–166.96 s), and the left contact angle increases while the right contact angle almost constant, as the bigger spindle has a larger capillary adhesion force. As a control experiment, water droplets do little transport on uniform spindle-knot fiber (Supplementary Fig. S4). In terms of critical hanging-drop volume before detached off versus time, it is estimated in efficiency of water collection that the GSFs are ~ 509.4 µl/h, which are much higher than that (~ 156.7 µl/h) of uniform spindle-knots fiber. It is demonstrated that GSF allows the drops (e.g., water, isooctane) to move along the gradient spindle-knots from the small one to the big one as target and also realizes the liquid collection in directionality (see supplementary Fig. S5)

We analysis that such transport is attributed to two main aspects to form the driving force (as illustrated in Fig. 3c-d): 1) the force (f_l) from the difference of the Laplace pressure [22,27] along the gradient spindle-knots as follows:

$$f_l = -\int_{r1}^{r2} \frac{2\gamma}{(r+R)2} \sin\beta \, dz \qquad (1)$$

Where γ is the surface tension of liquid, r is the local radius, R is the drop radius, β is the half apex-angles of the spindle-knots (among $\beta_{\text{(big knot)}} > \beta_{\text{(small knot)}}$); and z is the integrating variable along the height of the gradient spindle-knots. The Laplace pressure on the high curvature site (the minimum diameter of fiber with local radius, r_1) is larger than that on the low curvature site (the spindle-knot with local radius, r_2), where r_1 is smaller than r_2. Because $r_{1\text{(small knot)}} = r_{1\text{(large knot)}}$, $r_{2\text{(small knot)}} < r_{2\text{(large knot)}}$, then $f_{l\text{ (small knot)}} > f_{l\text{ (big knot)}}$, the non-equilibrium Laplace pressure will propel the water drop to move from the small knot to the big knot. 2) Capillary adhesion force (f_c), is considered to enhance with increasing geometric features of the spindle-knots along the fiber [28–29]. Given by:

$$f_c = 2\int_{xl}^{xl+d} \gamma \Phi(x) dx \qquad (2)$$

where x is the coordinate variable along the fiber axially, x_l is the initial site for the integration located at the outer ends of the left spindle-knot, d is the distance between two adjacent knots outer ends, and $\Phi(x)$ is the local crossing angle between the liquid surface and the vertical reference plane along the fiber. As d is proportional to the knot size, larger spindle-knot has larger d, so $f_{c\text{ (small knot)}} < f_{c\text{ (big knot)}}$. It is inferred that the geometry gradient of spindle-knots induces the gradient of capillary adhesion force, thus drops shift toward the larger-sized spindle-knot[28]. Based on the both factors above, the total force (F) can be described as：

$$F \sim f_l + f_c \qquad (3)$$

The overall result is that droplets directionally coalesce from joint to spindle-knot, and continuous coalescence induces droplet transport from small spindle-knot to big one, and target transport is controlled by biggest spindle-knot (Fig. 3d). To further demonstrate the controlling of droplet target transport, we observe the GSFs with the continuous gradient-step spindle-knots

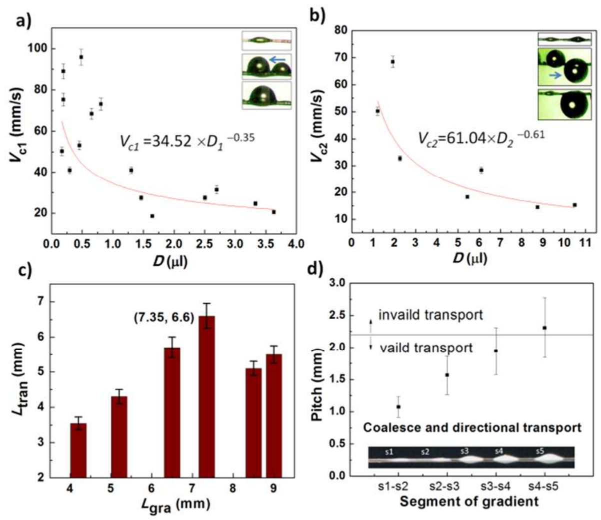

Fig. 4 The micro-droplet dynamic coalescence and transport behavior on GSFs. (a) The relationship between coalescence velocity (V_{c1}) and droplet volume (D_1) on single spindle. There is linear relationship V_{c1}=34.52× $D_1^{-0.35}$ by fitting. **(b)** The relationship between coalescence velocity (V_{c2}) and droplet volume (D_2) on two adjacent spindle-knots, there is V_{c2}=61.04× $D_2^{-0.61}$ by fitting. Micro-droplets coalesce fast on adjacent spindle (b) than single spindle (a) (micro-droplet with volume of 1–3 µl). **(c)** Bargraph of L_{tran} versus L_{gra} on GSF with unidirectional mode. The L_{gra} ranged in ~ 4–9 mm can make droplet move L_{tran} ranged in ~ 3.0–6.6 mm. The maximum L_{tran} is ~ 6.6 mm along the L_{gra} of ~ 7.35 mm (highest bar). **(d)** The chart of pitch of five spindle-knots (marked with s1, s2, s3, s4, and s5) on segments of gradient (s1-s2, s2-s3, s3-s4, s4-s5) on the fiber. The abscissa presents the four pitches successively from the samllest knot to the largest knot (as shown in the inset). When the pitch < 2.2 mm, water droplet can coalesce direcitonally, while pitch > 2.2 mm, droplet transport is invaild. Pitch is the center distance of two adjacent spindle-knots.

on a large scale including three periodicities (see supplementary Fig. S6), where droplet still transports to target that is controlled by large size spindle-knot in every gradient segment.

To highlight the droplet transport property, droplet's coalescence velocity (V_c) with droplet volume (D) is analyzed further. **Figure 4**a-b show the micro-droplet coalescence velocity on the single spindle and two adjacent spindles. Both on the two styles of spindles, V_c decreases with D increasing. On the single spindle-knot (height ~ 300 μm, width ~ 980 μm), the smallest micro-droplet (~ 0.19 μl) has a large coalescence velocity (~ 90 mm/s). When the D_1 is smaller than ~ 0.75 μl, V_{c1} decreases sharply from ~ 95 mm/s to ~ 40 mm/s, as for micro-droplet, its volume has an important impact on its coalescence velocity. But D_1 is a little larger at ~ 1.5–3.7 μl, the V_{c1} is among ~ 20–30 mm/s. There is a linear relationship between V_{c1} and D_1, i.e., $V_{c1}=34.52\times D_1^{-0.35}$ (Fig. 4a). To clarify how the gradient impacts on the micro-droplet coalescence velocity, we choose two adjacent spindles (with size ratio of 3.4:1), when $D_2 < 4$ μl, there is $V_{c2} > 30$ mm/s ($>V_{c1}$ above) as Laplace pressure existing between spindles is the driving force. As shown in Fig. 4b, there is the relationship between V_{c2} and D_2, i.e., $V_{c2}=61.04\times D_2^{-0.61}$. It is estimated that $V_{c2,\ max} \sim 70$ mm/s for $D_2 \sim 2$ μl, and the $D_{2\ max} \sim 11$ μl with a $V_{c2} \sim 15$ mm/s. Apparently, it implies that droplet with larger volume tends to move its mass-centre off main-axis fiber as collecting task, and also the tiny droplet transport is high efficient along the gradient of GSF. In addition, the transport length (L_{tran}) of droplets is relied on the L_{gra} of spindle-knots. As shown in Fig. 4c, it is found that when $L_{gra} < 7.35$ mm, the L_{tran} increases signficantly. But $L_{gra} > 7.35$ mm, the L_{tran} decreases. Fig. 4d shows the relationship of the pitches between spindle-knots (marked with s1, s2, s3, s4 and s5) on GSF. As the spindle-knots are bigger, the pitches between them would be longer. If the pitch of spindle-knots is more than 2.2 mm, the adjacent two droplets can not coalesce for further transport, so $L_{gra} > \sim 7.35$ mm, the L_{tran} decrease. Based on these of Fig. 4c-d, we can screen GSF on which droplets transport with different modes realising target transport via controllable experiment parameters in fabrication (see supplementary Fig. S2 and Fig. S7) so that GSF can achieve an excellent target transport in a range of ~ 6.6 mm for a gradient length of ~ 7.35 mm for optimal GSF with uni-directional modes. As for an improved transport in range (such as $L_{gra} > \sim 7.35$ mm), surfaces of fibers need to be further designed, e.g., adding sub-spindle-knots between pitches of main spindle-knots,[30] or chemical-treated gradient[1] so as to supply fluctuation of capillary to maintain a continuous transport in macro-level. Some works are going on.

Droplet target transport is further modulated by fabricating GSFs with various gradient modes (Supplementary Fig. S8 and table S1). The GSFs with middle and two-side symmetric gradient modes can achieve other styles intersting droplet target transport, in addition to the uni-direction gradient mode above (Fig. 3). **Figure 5**a shows droplet transport on GSF with middle symmetric gradient mode. At ~ 24.1 s, there is a droplet on every spindle-knot, respectively. Subsequently, droplet 5 and 4 coalesce into droplet (4+5), and droplet 1, 2 and 3 coalesce into a droplet (1+2+3). Finally, droplet (4+5) and droplet (1+2+3) gather into droplet (1+2+3+4+5) at ~ 117.0 s (Fig. 5a). All the water droplets directionally move from small spindle-knot to big spindle-knot, target the middle location to form a large drop, as the driving force $F_{smaller} < F_{small} < F_{big} > F_{small} > F_{smaller}$ (Fig. 5b). As for the droplet transport on GSF with two-side symmetric gradient mode (Fig. 5c). There are six droplets on the GSF after ~ 18.2 s. Subsequently, droplet 4, 5 and 6 coalesce into drop (4+5+6), and droplet 1, 2 and 3 coalesce into a droplet (1+2+3). Droplets transport separately, i.e., droplet (4+5+6) and droplet (1+2+3) target transports to each end of the GSF, via the force relationship at left: $F_{big} > F_{small} > F_{smaller}$ and at right: $F_{smaller} < F_{small} < F_{big}$ (Fig. 5d). It indicates that the as-designed GSF can regulate effectively the droplet target transport by size effect.

In summary, a unique size-triggered microdroplet target transport is achieved on GSFs those are fabricated controllably by developing a velocity-changed coating method. The GSFs achieve an excellent droplet target transport in directions regulated by the spindle-knot sized ditributions to form uni-directional, middle or two-side symmetric modes where are fabricated by controlling changes of drawing velocities. The finding offers a novel insight into the design of gradient fiber for multi-functions, and opens a way to effectively control liquid self-transport in directions, and also is significant to design the materials with water collection function in effciency, and also would be extended into relams of smart materials, e.g., fluid-controlling in some applcations[31–33].

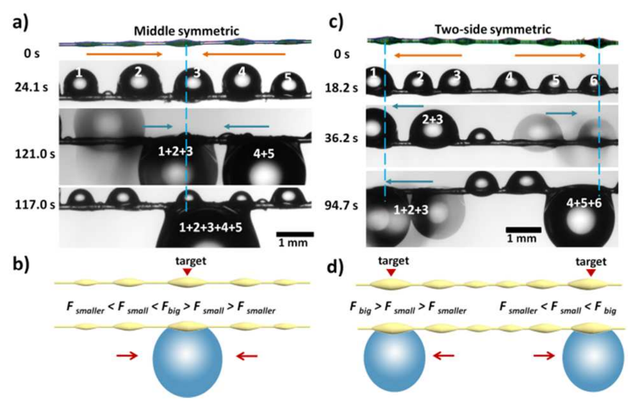

Fig. 5 Optical images of droplet transport on GSFs with middle symmetric and two-side symmetric gradient modes. **(a)** The middle symmetric gradient mode: At ~ 24.1 s, the droplet 1,2,3,4, and 5 form on every spindle-knot, respectively. Subsequently, droplet 1,2,3 coalesce into droplet (1+2+3), droplet 5, 4 coalesce into droplet (4+5) at ~ 121.0 s, respectively. Finally, droplet (4+5) and droplet (1+2+3) form droplet (1+2+3+4+5) at ~ 117 s, targets at middle of GSF, i.e., the location of big spindle-knot. **(b)** Illustration of middle symmetric gradient mode: the cooperative force relationship: $F_{smaller} < F_{small} < F_{big} > F_{small} > F_{smaller}$, the droplet targets at big spindle-knot. **(c)** The two-side symmetric gradient mode: At ~18.2 s, droplet 1,2,3,4,5 and 6 form on gradient-step spindle-knot, respectively. Subsequently, droplet 2,3 coalesce into droplet (2+3), and droplet 4, 5 and 6 coalesce into droplet (4+5+6) at ~ 36.2 s. Finally, droplet (2+3) and droplet 1 coalesce directionally into (1+2+3) at location of the left bigger spindle-knot, and droplet (4+5+6) target at location of the right bigger spindle-knot at ~ 94.7 s. The separated style of droplet transport appears on GSF with two-side symmetric gradient mode. Arrows represent the direction of the droplet transport. **(d)** Illustration of two-side symmetric gradient mode: the cooperative force relationship: left: $F_{big} > F_{small} > F_{smaller}$; right: $F_{smaller} < F_{small} < F_{big}$, the droplets separately target at two side big spindle-knots. Scale bars are 1 mm.

This work is supported by National Natural Science Foundation of China (21234001), National Key Basic Research Program of China (2013CB933000), Doctoral Fund of Ministry of Education of China (20121102110035).

Notes and references

[a]*Key Laboratory of Bio-Inspired Smart Interfacial Science and technology of Ministry of Education, School of Chemistry and Environment, Beihang University, Beijing 100191, P. R. China.*
E-mail: zhengym@buaa.edu.cn
[b]*Beijing National Laboratory for Molecular Sciences (BNLMS), Institute of Chemistry, Chinese Academy of Sciences, Beijing 100190, P. R. China.*

1 S. Daniel; M. K. Chaudhury; J. C. Chen: *Science* 2001, **291**, 633–636.
2 J. Zhang; Y. Han: *Langmuir* 2007, **23**, 6136–6141.
3 S. Mettu; M. K. Chaudhury: *Langmuir* 2008, **24**, 10833–10837.
4 S. Daniel; M. K. Chaudhury: *Langmuir* 2002, **18**, 3404–3407.
5 X. Han; L. Wang; X. Wang: *Adv. Funct. Mater.* 2012, **22**, 4533–4538.
6 J. Ju; H. Bai; Y. Zheng; T. Zhao; R. Fang; L. Jiang: *Nat. Commun.* 2012, **3**, 1247.
7 H. Mooney; P. Weisser; S. Gulmon: *Flora* 1977, **166**, 117–124.
8 R. Schill; W. Barthlott; N. Ehler: *Cact. Succ. J.* 1973, **45**, 175–185.
9 A. Mosco: *Revista Mexicana de Biodiversidad* 2009, **80**, 119–128.
10 Y. Zheng; H. Bai; Z. Huang; X. Tian; F. Q. Nie; Y. Zhao; J. Zhai; L. Jiang: *Nature* 2010, **463**, 640–643.
11 X. Tian; H. Bai; Y. Zheng; L. Jiang: *Adv. Funct. Mater.* 2011, **21**, 1398–1402.
12 Y. Liu; Z. Shao; F. Vollrath: *Nat. Mater.* 2005, **4**, 901–905.
13 Y. Yang; X. Chen; Z. Shao; P. Zhou; D. Porter; D. P. Knight; F. Vollrath: *Adv. Mater.* 2005, **17**, 84–88.
14 H. Bai; J. Ju; R. Z. Sun; Y. Chen; Y. M. Zheng; L. Jiang: *Adv. Mater.* 2011, **23**, 3708–3711.
15 H. Bai; X. L. Tian; Y. M. Zheng; J. Ju; Y. Zhao; L. Jiang: *Adv. Mater.* 2010, **22**, 5521–5525.
16 Y. Hou; Y. Chen; Y. Xue; Y. Zheng; L. Jiang: *Langmuir* 2012, **28**, 4737-4743.
17 H. Bai; R. Z. Sun; J. Ju; X. Yao; Y. M. Zheng; L. Jiang: *Small* 2011, **7**, 3429–3433.
18 H. Dong; N. Wang; L. Wang; H. Bai; J. Wu; Y. M. Zheng; Y. Zhao; L. Jiang: *Chem.phys.chem* 2012, **13**, 1153–1156.
19 E. Kang; G. S. Jeong; Y. Y. Choi; K. H. Lee; A. Khademhosseini; S.-H. Lee: *Nat. Mater.* 2011, **10**, 877–883.
20 D. Quéré: *Annu. Rev. Fluid Mech.* 1999, **31**, 347–384.
21 J. A. Diez; R. Gratton; L. P. Thomas; B. Marino: *Physics of Fluids* 1994, **6**, 24–33.
22 M. Deserno: *J. Phys. Chem. E* 2001, **6**, 163–168.
23 D. Quéré: *EPL (Europhysics Letters)* 2007, **13**, 721.
24 D. Quéré; J. M. di Meglio; F. Brochard-Wyart: *Science* 1990, **249**, 1256–1260.
25 Y. Chen; L. Wang; Y. Xue; L. Jiang; Y. Zheng: *Sci. Rep.* 2013, **3**, 2927.
26 L. Lorenceau; D. Qur: *J. Fluid. Mech.* 2004, **510**, 29–45.
27 X. L. Tian; Y. Chen; Y. M. Zheng; H. Bai; L. Jiang: *Adv. Mater.* 2011, **23**, 5486–5491.
28 Z. Huang; Y. Chen; Y. Zheng; L. Jiang: *Soft Matter* 2011, **7**, 9468–9473.
29 É. Lorenceau; C. Clanet; D. Quéré: *J.Colloid Interf. Sci.* 2004, **279**, 192–197.
30 Y. Chen; L. Wang; Y. Xue; Y. Zheng; L. Jiang: *Soft Matter* 2012, **8**, 11450 –11454.
31 F. Benito-Lopez; R. Byrne; A. M. Răduţă; N. E. Vrana; G. McGuinness; D. Diamond: *Lab on a Chip* 2010, **10**, 195–201.
32 S. Hosseini; H. V. Tafreshi: *Powder Technol.* 2011, **212**, 425–431.
33 H. Bai; J. Ju; Y. Zheng; L. Jiang: *Adv. Mater.* 2012, **24**, 2786–2791.

Cite this: DOI: 10.1039/c0xx00000x

www.rsc.org/xxxxxx

COMMUNICATION

Text of highlight

Directional size-triggered microdroplet target transport is achieved on gradient-step fiber due to continuous capillary gradient cooperative effect.

Color graphic: